

Vacuum polarization and Wichmann-Kroll correction in the finite basis set approximation

V. K. Ivanov,^{1,*} S. S. Baturin,¹ D. A. Glazov,¹ and A. V. Volotka¹

¹*School of Physics and Engineering, ITMO University, 197101 St. Petersburg, Russia*

(Dated: June 12, 2024)

The finite basis set method is commonly used to calculate atomic spectra, including QED contributions such as bound-electron self-energy. Still, it remains problematic and underexplored for vacuum-polarization calculations. We fill this gap by trying this approach in its application to the calculation of the vacuum-polarization charge density and the Wichmann-Kroll correction to the electron binding energy in a hydrogen-like ion. We study the convergence of the method with different types and sizes of basis sets. We cross-check our results for the Wichmann-Kroll correction by direct integration of the Green's function. As a relevant example, we consider several heavy hydrogen-like ions and evaluate the vacuum polarization correction for S and P electron orbitals.

I. INTRODUCTION

Quantum electrodynamics (QED) is one of the most established and well-developed field theories. Extensive experimental tests show a high predictive power of this theory and an almost extreme accuracy. The latter is due to smallness of the fine-structure constant $\alpha \approx 1/137$, which is the coupling constant of the theory. To date, many experimental tests of QED have been performed. However, there is still considerable interest and development when it comes to QED in strong electromagnetic fields. Such processes reveal tiny effects that are not observed in the regular scenario and allow testing QED with much higher precision. In highly charged heavy ions, it is remarkable that the electric field is only a few orders smaller than the Schwinger limit. For example, the surface field of the Uranium nucleus is $\sim 10^{19}$ V/cm. This makes highly charged heavy ion a perfect system for testing the strong field QED.

To perform these tests and to compare theory with experiment, a precise calculation of the lowest electron level binding energies is required. A natural approach to the analysis of different systems within QED is the perturbation series, which could be evaluated with some effort to a high order in small parameter α and thus to a high degree of accuracy. While algorithms exist to perform such calculations, many of them require significant computational resources, especially when it comes to the evaluation of the higher order terms. Optimization and improvement of the computational methods and algorithms as well as increasing the computational speed is one of the prominent research directions.

Development of such algorithms becomes especially important to calculate QED effects in systems in the strong field regime. In such systems the high-precision QED calculations become complex since the parameter, by which an electron is coupled to the external field, may be large. For instance, in the presence of a heavy nucleus,

the electrons are coupled to the external field through the factor $Z\alpha$, where Z is the atomic number – this coupling constant is not sufficiently small when considering heavy elements with $Z \sim 100$. For such systems, the contribution of higher-order terms in the $Z\alpha$ expansion becomes too large, thus perturbative methods, mentioned above, cannot be used. [1]. To address this issue, it is necessary to employ the non-perturbative approach, known as the Furry's picture, in which the external field of the nucleus is incorporated into the electron wave function.

In this work, we focus on the vacuum polarization effect (Fig. 1), which along with the one-photon exchange (relevant for atoms with more than one electron) and the self-energy diagrams consist the main QED contributions to atomic spectrum. Vacuum polarization (VP) can be thought of as the creation of a virtual electron-positron pair under the influence of the strong nuclei potential on the Dirac sea. This interaction effectively attracts the electron part of the electromagnetic vacuum while pushing away the positron part. As a consequence of the aforementioned local charge imbalance, the nucleus field is effectively screened. VP leads to a Lamb shift in the atomic spectrum [1, 2] and, together with other types of QED contributions, constitutes an indispensable component of the g -factor calculation [3–6]. The calculations of the g -factor of highly charged ions are currently being actively explored [7], as they have a number of important applications. These include the precise determination of the electron mass by studying hydrogen-like ions [8], as well as a possible independent test for the value of the fine-structure constant [9, 10]. In addition to hydrogen-like ions, systems with a larger number of electrons are being considered. These include highly charged two-electron ions [11] and beryllium-like ions [12]. Furthermore, vacuum polarization with more than one loop [2] is of interest.

In the leading order in $Z\alpha$, the VP contribution induces the Uehling potential. It provides the major part of the energy shift in the atomic spectrum originating from vacuum polarization (see, for example, [13]). For heavy elements, higher orders in $Z\alpha$ expansion become significant. The $\alpha(Z\alpha)^3$ contribution was calculated by Wich-

* E-mail: vladislav.ivanov@metalab.ifmo.ru

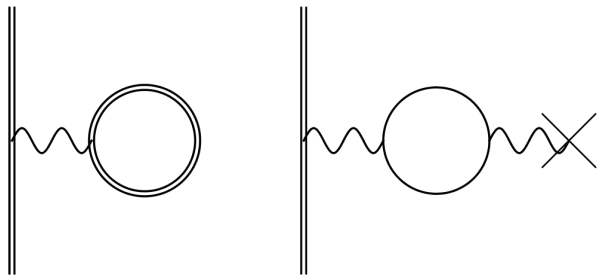


Figure 1. Vacuum polarization diagrams. Left: vacuum polarization in Furry's picture, all orders of $\alpha(Z\alpha)$ are included. Right: the Uehling correction. Double lines denote an electron in an external field, single straight lines are free electron propagators, cross is the external field source, wavy lines denote a propagating photon.

mann and Kroll [14], and later in [15], many-potential contribution from $\alpha(Z\alpha)^{n \geq 3}$ was also found. The importance of the Wichmann-Kroll vacuum polarization effect become apparent for heavy hydrogen-like ions, for which the VP Lamb shift is on the order of eV [1, 13].

In the present study, we evaluate the VP charge density using the finite basis set (FBS) approximation. This approach has already been used for electron self-energy diagrams [16]. We take the next step and explore its applicability and accuracy in connection to vacuum polarization. The standard approach to these diagrams is to integrate the Green's function directly, which is a time-consuming and complicated procedure. The first step towards developing this procedure was discussed in [17], where the FBS method was applied to evaluate the vacuum polarization density on a Gaussian basis set. We build on these findings by testing the FBS method with both the Gaussian basis set and the B-spline basis set. The latter is widely used for self-energy diagrams. We calculate the induced charge density for various partial wave contributions up to the value of $|\kappa| = 5$ and obtain the corresponding Wichmann-Kroll corrections for the electron energy levels of several hydrogen-like ions.

Throughout this paper, we use a natural unit system $\hbar = c = m = 1$.

II. BASIC THEORY

A. Radial Dirac equation

We start from a single electron Dirac equation that has the form:

$$(\gamma^\mu p_\mu - m)\psi = 0, \quad (1)$$

where γ^μ are the Dirac gamma matrices, p_μ is the four-momentum of the electron, and m is the electron mass.

Further, we assume $m = 1$. For a free electron, p_μ is the kinetic momentum p_{kin} , and for an electron in an external field, $(p_{\text{kin}} - eA)$, where e is the electron charge and A is the external photon field potential.

For the fermionic field operator, we can write

$$\psi(x) = \sum_{E_n > 0} a_n \phi_n(x) + \sum_{E_n < 0} b_n^\dagger \phi_n(x), \quad (2)$$

where a_n, b_n^\dagger are the annihilation/creation operators for an electron/positron and $\phi_n(x)$ are fermionic wave functions. We assume the spectrum to be discrete, which is customary in bound-state QED calculations.

For time-independent problem of an electron in an external electric field, the Dirac equation for the wave functions $\phi_n(x)$ can be written in the following form:

$$h_D \phi_n(x) = E_n \phi_n(x), \quad (3)$$

where the Hamiltonian h_D is expressed as

$$h_D = -i\alpha\nabla + \beta + V(\mathbf{x}), \quad (4)$$

$$\beta = \gamma^0, \quad \alpha = \gamma^0\gamma. \quad (5)$$

Here, ∇ is a standard nabla operator, and $V(x)$ is the external field potential (the potential of the nucleus in our case).

Stationary solutions to the Dirac equation can be expressed as

$$\phi_n(x) = \phi_n(\mathbf{x})e^{-iE_n t}. \quad (6)$$

For a spherically symmetric problem, we can perform a separation of variables and achieve a radial Dirac equation for the radial component of wave functions (3), which also provides the electron energy spectrum. To separate the variables, we choose the wave function in the form

$$\phi_n(\mathbf{x}) = \frac{1}{r} \begin{bmatrix} P_{n,\kappa}(r)\Omega_{\kappa,m}(\theta, \varphi) \\ iQ_{n,\kappa}(r)\Omega_{-\kappa,m}(\theta, \varphi) \end{bmatrix}, \quad (7)$$

where κ is the relativistic angular quantum number, related to the total and orbital momenta as $j = |\kappa| - \frac{1}{2}$ and $l = |\kappa + \frac{1}{2}| - \frac{1}{2}$, respectively. The description of spherical spinors $\Omega(\theta, \varphi)$ can be found, for example, in [1, 18, 19]. We substitute the ansatz (7) into the Dirac equation (3), and arrive at the radial Dirac equation:

$$\begin{bmatrix} m + V & -\frac{d}{dr} + \frac{\kappa}{r} \\ \frac{d}{dr} + \frac{\kappa}{r} & -m + V \end{bmatrix} \begin{bmatrix} P_{n,\kappa} \\ Q_{n,\kappa} \end{bmatrix} = E_n \begin{bmatrix} P_{n,\kappa} \\ Q_{n,\kappa} \end{bmatrix}. \quad (8)$$

The equation above has an analytic solution in the case of the Coulomb potential [18]. For an arbitrary potential, one can still proceed numerically. Variational methods are the most common choice for numerical solutions. In Section III, we provide one of the numerical approaches, which we then apply to the calculation of the vacuum polarization calculation method.

B. Vacuum polarization

The VP charge density can be derived directly from the fermionic current operator. The expression for the current operator reads [20]

$$j^\mu(x) = \frac{e}{2} [\bar{\psi}(x)\gamma^\mu, \psi(x)]. \quad (9)$$

This expression originates from the charge symmetrization and is typical for bound-state QED. The induced

$$\Delta E_n = 4\pi i\alpha \int d(t_2 - t_1) \int d^3x_2 \int d^3x_1 \bar{\phi}_n(x_2) \gamma^\mu \phi_n(x_2) D_F(x_2 - x_1) \text{Tr}[\gamma_\mu S_F(x_1, x_1)], \quad (10)$$

where

$$D_F(x_2 - x_1) = -i \int \frac{d^4k}{(2\pi)^4} \frac{e^{-ik(x_2 - x_1)}}{k^2 + i\varepsilon} \quad (11)$$

is the photon propagator, and the fermion propagator is defined as

$$\begin{aligned} S_F(x_2, x_1) &= \langle 0 | T \{ \psi(x_2) \bar{\psi}(x_1) \} | 0 \rangle \\ &= \begin{cases} \sum_{E_n > 0} \phi_n(x_2) \bar{\phi}_n(x_1), & t_1 < t_2 \\ - \sum_{E_n < 0} \phi_n(x_2) \bar{\phi}_n(x_1), & t_1 > t_2 \end{cases} \\ &= \frac{1}{2\pi i} \int_{C_F} dz \sum_n \frac{\phi_n(\mathbf{x}_2) \bar{\phi}_n(\mathbf{x}_1)}{E_n - z(1 + i\delta)} e^{-z(t_2 - t_1)} \\ &= \frac{1}{2\pi i} \int_{C_F} dz G(\mathbf{x}_2, \mathbf{x}_1, z(1 + i\delta)) \gamma^0 e^{-z(t_2 - t_1)}. \end{aligned} \quad (12)$$

Above, $G(\mathbf{x}_2, \mathbf{x}_1, z(1 + i\delta))$ is the Green's function of the time-independent Dirac equation (3), and $\phi_n(x)$ are the solutions in the external field. The second line of (12) is used in our FBS method, while the last two lines are used for the direct integration method [1, 21].

We evaluate integrals in (10) and, assuming that the system is stationary, find the energy correction to the j -th electron energy level:

$$\Delta E_j = \int d^3x_1 \phi_j^\dagger(\mathbf{x}_1) U(\mathbf{x}_1) \phi_j(\mathbf{x}_1), \quad (13)$$

$$\begin{aligned} U(\mathbf{x}_2) &= \frac{i\alpha}{2\pi} \int d^3x_1 \frac{1}{|\mathbf{x}_1 - \mathbf{x}_2|} \int_{C_F} dz \text{Tr} G(\mathbf{x}_1, \mathbf{x}_2, z) \\ &= \frac{i\alpha}{2\pi} \int d^3x_1 \frac{1}{|\mathbf{x}_1 - \mathbf{x}_2|} \text{Tr}[\gamma_0 S_F(x_1, x_1)]. \end{aligned} \quad (14)$$

charge density can be found as the timelike component of this current (See [14]), if we consider the solutions for wave functions in an external field (4-5). However, here, we shall find the same result with a more general approach, i.e. from the scattering amplitude, using the expression for the energy correction from [1, 21]. Later, we shall employ this expression to calculate the Wichmann-Kroll correction. With the help of the left diagram in Fig. 1 and Feynman rules for bound-state QED, we obtain the expression for the energy correction to the n -th level electron associated with the vacuum polarization:

We compare equation (14) with the Coulomb law

$$U(\mathbf{x}) = -e \int d^3x' \frac{\rho(\mathbf{x}')}{|\mathbf{x} - \mathbf{x}'|}, \quad (15)$$

and finally, obtain the expression for the induced charge density [14, 20]:

$$\begin{aligned} \rho(\mathbf{x}) &= ie \text{Tr}[S_F(x, x') \gamma_0] |_{x \rightarrow x'} \\ &= \frac{ie}{2} \left(\sum_{E_n > 0} \phi_n(\mathbf{x}) \phi_n^\dagger(\mathbf{x}) - \sum_{E_n < 0} \phi_n(\mathbf{x}) \phi_n^\dagger(\mathbf{x}) \right). \end{aligned} \quad (16)$$

Above, $x \rightarrow x'$ should be understood as an average over the limits from the left and from the right [1, 20]. On the other hand, if we start from the current (9), similar to [20], we find:

$$j^\mu(\mathbf{x}) = ie \text{Tr}\{S_F(x, x') \gamma^\mu\} |_{x \rightarrow x'}, \quad (17)$$

where the timelike component is, once again, the charge density.

III. FINITE BASIS SET APPROXIMATION

One of the approaches to the variational problem for the radial Dirac equation is the Ritz-Rayleigh or Ritz-Galerkin method. The idea is to use the finite set of basis functions, and approximate the solution to the Dirac equation as a sum of these functions with weight coefficients found from a variation problem. The energy spectrum is found as a byproduct of this procedure.

A. Variational method

The core of the finite basis method is the approximation of the exact solution to the radial Dirac equation

with the weighted sum over a finite set of some basis functions. Unknown coefficients in this sum are found with the help of variational methods [19, 22–25].

In this method, the energy expectation value (or action in some papers, alternatively) is expressed using the “test” wave function, defined as the sum over the given finite basis functions with unknown coefficients. Next, these coefficients are found by variation of the energy expectation value [26] (or the action [24]).

Let us define the test function next way:

$$\Psi(r) = \sum_{i=1}^n v_i \pi_i(r), \quad (18)$$

where $\pi_i(r)$ are functions from some known finite basis set. The expectation value (or the Rayleigh quotient) for ε , which happens to be the upper bound for the true value of energy [26] reads:

$$\varepsilon = \frac{\langle \Psi | H | \Psi \rangle}{\langle \Psi | \Psi \rangle} = \frac{\sum v_i^* v_j H_{ij}}{\sum v_i^* v_j C_{ij}}. \quad (19)$$

We vary the coefficients and require the variation of the energy expectation value to be minimal. Varying ε , we obtain

$$\frac{\partial \varepsilon}{\partial v_k^*} = \frac{\sum v_j H_{kj}}{\sum v_i^* v_j C_{ij}} - \frac{\sum v_i^* v_j H_{ij} \sum v_j C_{kj}}{(\sum v_i^* v_j C_{ij})^2} \quad (20)$$

$$= \frac{\sum v_j (H_{kj} - \varepsilon C_{kj})}{\sum v_i^* v_j C_{ij}}. \quad (21)$$

To obtain the minimum, these derivatives (21) should be equal to zero, which leads to secular equations:

$$v_j (H_{kj} - \varepsilon C_{kj}) = 0, \quad (22)$$

or, in matrix form:

$$\mathbf{H}\mathbf{v} = \varepsilon \mathbf{C}\mathbf{v}. \quad (23)$$

Above, we recognize a generalized eigenvalue problem with hermitian matrices \mathbf{H} and \mathbf{C} , where ε are the upper bounds for the Dirac equation spectrum, and v are eigenvectors, consisting of coefficients involved in the sum that defines the wave functions (18). With the increase in the size of the basis set, the approximate spectrum values ε (and the wave functions calculated using the obtained coefficients) become closer to their true values. [27]

In the case of the radial Dirac equation (8), we solve for the “large” and “small” components of the wave function, therefore, we define two sums:

$$P_\kappa = \sum_{i=1}^n p_i \pi_i^+(r) \quad (24)$$

$$Q_\kappa = \sum_{i=1}^n q_i \pi_i^-(r), \quad (25)$$

where π_i^\pm are two basis sets, which could be identical or different, depending on the researcher’s choice. With this definition, \mathbf{H} can be written in the following form:

$$\mathbf{H} = \begin{pmatrix} \mathbf{H}^{LL} & \mathbf{H}^{LS} \\ \mathbf{H}^{SL} & \mathbf{H}^{SS} \end{pmatrix} \quad (26)$$

where L, S stands for “large” and “small” components. For instance, for the first quadrant, we have

$$H_{ij}^{LL} = \int_0^\infty \pi_i^+(r) \pi_j^+(r) (m + V(r)) dr, \quad (27)$$

and analogously for the other quadrants. For the correct solution, we need to take into account boundary conditions [24, 25]. This can be done by adding a special term to the matrix \mathbf{H} [24], or by choosing basis functions that satisfy the boundary conditions for any set of coefficients (for example, equal to zero at $r = 0$ and ∞).

It is convenient to unite coefficients in P_κ, Q_κ like $v_i = (p_1, p_2, \dots, p_n, q_1, q_2, \dots, q_n)$ [24]:

$$P_\kappa = \sum_{i=1}^n v_i \pi_i^+(r) \quad (28)$$

$$Q_\kappa = \sum_{i=n+1}^{2n} v_i \pi_{i-n}^-(r) \quad (29)$$

B. Dual-kinetic balance

There is a well-known problem with the naïve choice of basis functions π^\pm (when the large and small components are independent) in the Dirac problem. Spurious nonphysical states emerge in the spectrum [28]. Such states can be ignored [25, 26]. However, it is more convenient to choose a basis set that mitigates these spurious states.

In the so-called kinetic balance (KB) approach, large component solutions are tied to the small components solutions: $\pi^+ = \frac{1}{2} \left(\frac{d}{dr} + \frac{\kappa}{r} \right) \pi^-$. However, this approach is asymmetrical for positive and negative energy terms, which can, for example, lead to a violation of \mathcal{C} -symmetry in vacuum polarization calculations [17]. In the alternative dual-kinetic balance (DKB) approach [16], positive and negative energy components are mixed symmetrically, and the approximate solution is written as (compare with (28, 29)):

$$\varphi_\kappa = \begin{bmatrix} P_\kappa \\ Q_\kappa \end{bmatrix} = \sum_{i=1}^n v_i \left[\frac{1}{2} \left(\frac{d}{dr} + \frac{\kappa}{r} \right) \pi_i^+ \right] + \sum_{i=n+1}^{2n} v_i \left[\frac{1}{2} \left(\frac{d}{dr} - \frac{\kappa}{r} \right) \pi_{i-n}^- \right]. \quad (30)$$

With DKB, for example, the overlap matrix in (23) becomes

$$\mathbf{C} = \begin{pmatrix} \mathbf{C}^{LL} & \mathbf{C}^{LS} \\ \mathbf{C}^{SL} & \mathbf{C}^{SS} \end{pmatrix}, \quad (31)$$

$$C_{ij}^{LL} = \int_0^\infty \pi_i^+ \pi_j^+ dr \quad (32)$$

$$C_{ij}^{LS} = \frac{1}{2} \int_0^\infty \pi_i^+ \left\{ \left(\frac{d}{dr} - \frac{\kappa}{r} \right) \pi_j^- \right\} dr \quad (33)$$

$$C_{ij}^{SS} = \frac{1}{4} \int_0^\infty \left\{ \left(\frac{d}{dr} - \frac{\kappa}{r} \right) \pi_i^- \right\} \left\{ \left(\frac{d}{dr} - \frac{\kappa}{r} \right) \pi_j^- \right\} dr \quad (34)$$

$$\mathbf{C}^{SL} = (\mathbf{C}^{LS})^T. \quad (35)$$

The expressions for \mathbf{H} matrix can be found similarly.

C. Induced charge density in the finite basis set approximation

Now we turn to the definition of the vacuum polarization charge density, using an FBS approach. In [17], it was suggested to calculate the induced charge density with the finite basis set approximation as follows: the charge density (16) is obtained as a sum of wave functions up to number $2n$, which are found by solving the Dirac equation.

In [14], it was shown that the vacuum polarization charge density can be decomposed into components with different angular momentum states:

$$\rho(\mathbf{x}) = \sum_{\kappa=\pm 1}^{\pm\infty} \rho_\kappa(\mathbf{x}) = \frac{e}{2\pi i} \int_{C_F} dz \sum_{\kappa=\pm 1}^{\infty} \frac{|\kappa|}{2\pi} \text{Tr} G_\kappa(\mathbf{x}_1, \mathbf{x}_2, z). \quad (36)$$

If the spectrum is assumed to be discrete, each of the ρ_κ components is defined as [17]

$$\rho_\kappa(\mathbf{x}) = \frac{|\kappa|}{2\pi} \frac{e}{2} \frac{1}{r^2} \sum_n \text{sgn}(E_{\kappa,n}) \rho_{\kappa,n}(r), \quad (37)$$

$$\rho_{\kappa,n}(r) = \varphi_{\kappa,n}^\dagger \varphi_{\kappa,n} = P_{n,\kappa}^2 + Q_{n,\kappa}^2. \quad (38)$$

For the exact solution, the sum in (37) should be infinite, but an approximate solution can be found with a finite basis set. In the latter case, the summation goes from $i = 1$ to $2n$, where n is the number of finite basis set functions.

The VP charge density contains divergent terms such as the Uehling term, which are often treated separately, since the renormalized expression for the Uehling potential is known [1]. To exclude this divergence, we expand the charge density in the powers of Z :

$$\rho_\kappa(r, Z) \equiv \sum_{k=0}^{\infty} \rho_\kappa^{(k)}(r, Z) = \sum_{k=0}^{\infty} \frac{\partial^k}{\partial Z^k} \rho_\kappa(r, Z) \Big|_{Z=0} \frac{Z^k}{k!}. \quad (39)$$

Here, $\rho_\kappa^{(1)}$ is the Uehling term, which contains linear divergence. Following [1, 21], we separate the finite part $\rho^{n \geq 3}$ by subtracting the diverging terms from the total induced charge density. Apart from the Uehling term, there is a spurious diverging piece in the third-order term $\tilde{\rho}^{(3)}$, which should also be considered:

$$\rho^{n \geq 3} = \rho - \rho^{(1)} - \tilde{\rho}^{(3)} \quad (40)$$

However, since we sum over finite number of angular momentum terms, the $\tilde{\rho}^{(3)}$ part vanishes, as shown in, for example, [21]. Then, subtracting the linear term, we have [17, 29]

$$\rho_\kappa^{n \geq 3}(r, Z) = \rho_\kappa(r, Z) - \lim_{\delta \rightarrow 0} \frac{Z}{\delta} \rho_\kappa(r, \delta) \quad (41)$$

Moreover, as discussed in [17], \mathcal{C} -symmetry is important to obtain the correct numerical solution for VP charge density. If this symmetry is not ensured in the finite basis set calculation method, the results can be corrupted. To provide the \mathcal{C} -symmetry is obeyed, it can be enforced directly:

$$\rho_{\kappa,\mathcal{C}}(r, Z) = \frac{1}{2} (\rho_\kappa(r, Z) - \rho_\kappa(r, -Z)), \quad (42)$$

so that

$$\rho_{\kappa,\mathcal{C}}^{n \geq 3}(r, Z) = \frac{1}{2} (\rho_\kappa^{n \geq 3}(r, Z) - \rho_\kappa^{n \geq 3}(r, -Z)) - \frac{Z}{2\delta} (\rho_\kappa^{n \geq 3}(r, \delta) - \rho_\kappa^{n \geq 3}(r, -\delta)). \quad (43)$$

It was discussed in [17], that the KB basis generally violates the \mathcal{C} -symmetry, while the DKB basis does not. We shall use (43) in our calculations below.

D. Basis sets

In the finite basis approximation method, there are several basis sets commonly used for bound-state QED calculations. One of these is the B-spline basis, widely used for the self-energy diagrams [16]. However, this basis does not work well for the vacuum polarization calculations. We show it below.

The B-spline basis is defined as: [24, 25, 30]

$$B_{i,1}(x) = \begin{cases} 1, & t_i \leq x < t_{i+1} \\ 0, & \text{otherwise} \end{cases} \quad (44)$$

where $\{t_1, \dots, t_n\}$ are the knot points, and higher degree B-splines are defined by the recurrent formula:

$$B_{i,k}(x) = \frac{x - t_i}{t_{i+k} - t_{i+1}} B_{i,k-1}(x) + \frac{t_{i+k} - x}{t_{i+k} - t_{i+1}} B_{i+1,k-1}(x). \quad (45)$$

These functions are k -degree polynomials defined on a finite interval and equal to zero elsewhere. B-spline basis functions are well-suited for integrating using Gauss-Legendre quadrature, and linear dependency is not a serious problem in this basis.

Another basis set, widely used in quantum chemistry and atomic physics, is the Gaussian basis set with the following basis functions [17, 22, 31]:

$$\pi_i^\pm(r) = \mathcal{N} r^{d_\pm} e^{-\zeta_i r^2}, \quad (46)$$

where d_\pm are chosen to simulate the wave function behavior near $r = 0$ and defined depending on the type of the potential, and \mathcal{N} is the normalization factor. For point-like (Coulomb) potential, d_\pm would be equal to $\gamma = \sqrt{\kappa^2 - (Z\alpha)^2}$ [18], but for shell model of nucleus, the potential near $r = 0$ is constant, which corresponds to free-particle behavior ($Z = 0$), thus in this case, we have [19]

$$d_\pm = \left| \kappa \pm \frac{1}{2} \right| + \frac{1}{2}. \quad (47)$$

The coefficients ζ_i in (46) are generated to form a geometric sequence [31]:

$$\zeta_i = \zeta_1 (\zeta_n / \zeta_1)^{\frac{i-1}{n-1}}, \quad (48)$$

where $\zeta_{1,n}$ are the first and last coefficients, and n is the size of the basis set. The Gaussian basis is better suited for vacuum polarization calculations, as we shall show below. However, this basis is subject to the linear dependence problem, which makes increasing the basis set size problematic. We shall also discuss this issue below.

IV. RESULTS

In this section, we calculate the vacuum polarization charge density and the Wichmann-Kroll correction associated with this density for hydrogen-like levels of various heavy ions. We plot the VP-induced charge density and compare it to the results of [1, 21]. We also compare the obtained Wichmann-Kroll corrections with the corresponding results from [13].

A. Calculation of VP charge density

First, we calculated VP charge densities as a function of the distance from the nucleus r . To calculate this density, we need to sum over an infinite number of angular momentum components. However, for heavy elements, a sum over partial components κ converges fast enough, and the first few terms can be sufficient. Following [1], we denote

$$\rho_{|\kappa|} = \rho_{-\kappa} + \rho_{\kappa}. \quad (49)$$

In VP calculations, partial terms are taken in pairs $\rho_{-\kappa} + \rho_{\kappa}$ [1, 14], which is necessary for cancellation of the zero-potential contribution [13, 17].

In Figs. 2-7, we show VP densities calculated for hydrogen-like Uranium $Z = 92$ with the nuclear radius $r_n = 5.751$ fm used different basis sets. We use a shell-like nucleus model throughout this work, where the nucleus charge density is modeled by

$$\rho_n(r) = \delta(r - r_n). \quad (50)$$

This nucleus model was used in [1, 17]; it is simple and provides a better behavior of the induced charge density near $r = 0$ than a point-like charge with $\rho_n(\mathbf{x}) = \delta(\mathbf{x})$.

We performed our calculations using both the B-spline and Gaussian basis sets. For the Gaussian basis, the matrices for the eigenvalue problem equation (23) can be calculated analytically for point- and shell-like potentials, which makes calculations more efficient and precise. We calculated these matrices using both analytical and numerical integration. For the B-spline basis set, these matrices were calculated using the Gauss-Legendre quadrature. We used parameters $\zeta_1 = (\frac{1}{386.159})^2 \times 10^3$ and $\zeta_n = (\frac{1}{386.159})^2 \times 10^{11}$, and the sizes of the Gaussian basis sets were chosen equal to 30 and 100. For the B-spline set, we used a basis set with 40 basis functions, and for knot values, we used a power grid with denser knots inside the nucleus.

There is a well-known problem associated with the Gaussian basis set (as opposed to the B-spline basis): as its size increases, the basis functions can become efficiently linearly dependent. This imposes an upper limit on the size of a Gaussian basis set; upon reaching this limit, the numerical solution collapses. This limit depends mainly on the numerical precision; thus, for our parameters, we can use only 30 basis functions if float numbers are used. This limit can be increased by using arbitrary precision numbers (at the expense of performance speed). We used 70-digit numbers for calculations with a set of 100 basis functions.

For our calculations, we used a Python program with mpmath package for multiple-precision calculations [32]. In Table I, we present the approximate evaluation time required for the calculation of $\rho_{|\kappa|}(r)$ for one value of

$|\kappa|$. The algorithm is quite time-efficient when machine-precision (`float`) numbers are used, while for arbitrary precision calculation, the required time is still tolerable (but a lot larger than for float, since symbolic calculations are used). [33]

Table I. Approximate time for the calculation of one $\rho_{|\kappa|}(r)$ term, for different number formats and sizes of the Gaussian basis set.

Basis set size, number format	Evaluation time, approximate
n=30, float	2 seconds
n=100, 70-digit multiple precision	10 minutes

Figures 2, 3 show the VP charge density calculated using a Gaussian basis set with $n = 30$. Here, the DKB method was applied. The radius scale is given in Compton wavelengths units $\lambda = \frac{1}{m}$. The presented plots are in good agreement with the results of [1, 17, 21] for $|\kappa| = 1$, which gives the major part of the total $\rho^{n \geq 3}$ and ΔE_{WK} value. However, there are noticeable oscillations, which spoil the charge density curves for higher values of $|\kappa|$ or, equivalently, for $r^2 \rho^{n \geq 3}$ smaller than $\approx 10^{-5}$. In Figs. 4, 5, we show calculation results for the same problem, but with the basis set size $n = 100$. Here, we do not use the DKB method, since imposing \mathcal{C} -symmetry by the rule (43) seems to be sufficient. Evidently, the results are much better this time, especially at a large distance from the nucleus. In Figs. 6, 7, we show VP plots calculated using the B-spline basis set. This time, the oscillations are significant for all curves corresponding to different orders in κ .

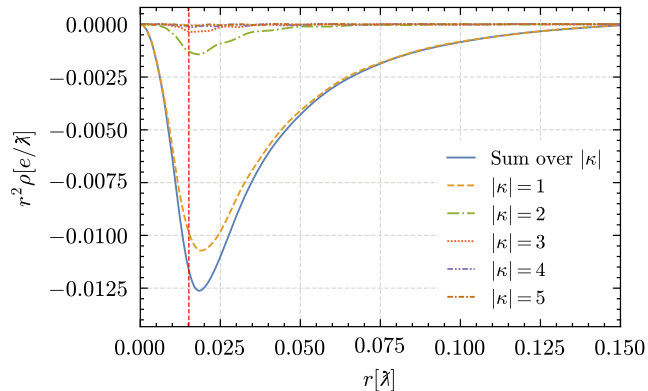


Figure 2. Radial vacuum polarization charge density of order $\alpha(Z\alpha)^{n \geq 3}$ for $Z = 92$ with nuclear radius $r_n = 5.751$ fm, at a small distance from the nucleus. Calculations were performed in Gaussian basis with the basis set size $n = 30$. Dashed lines: contributions from different κ ; solid line: sum over the first five contributions from different κ . A vertical line denotes the nuclear radius.

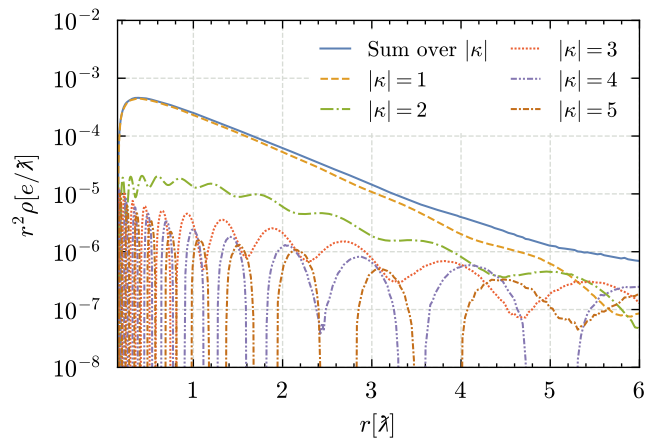


Figure 3. Same as Fig. 2, but in log-scale, at a large distance from the nucleus.

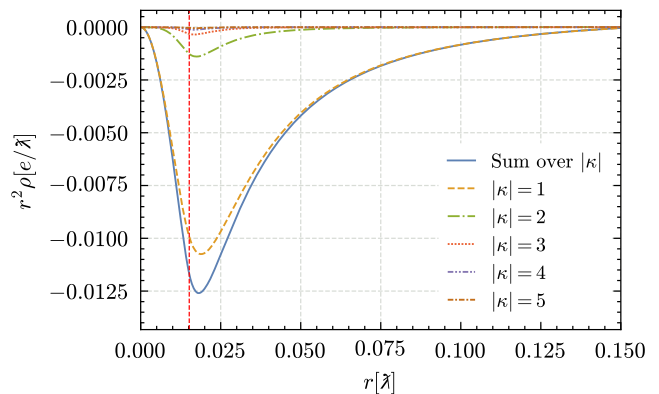


Figure 4. Same as Fig. 2, but with the basis set size $n = 100$.

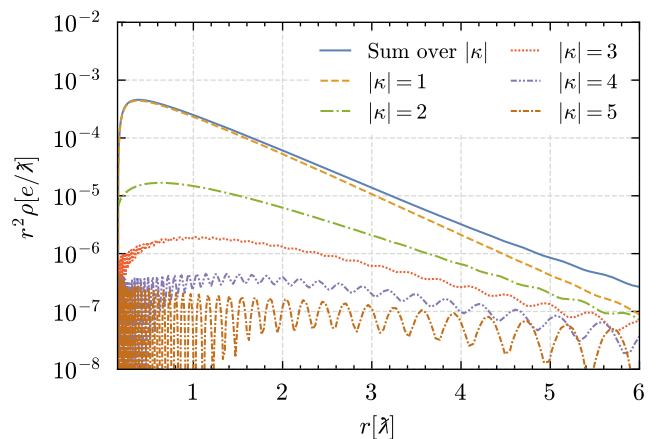


Figure 5. Same as Fig. 3, but with the basis set size $n = 100$.

B. Wichmann-Kroll correction

We have obtained the VP charge density, and now we can calculate the corresponding correction to the atomic

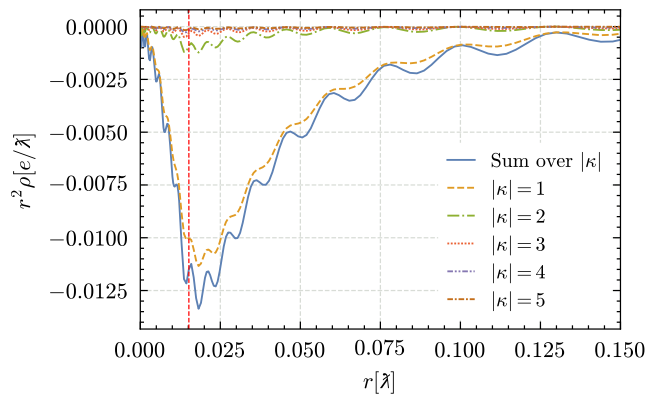


Figure 6. Radial vacuum polarization density of order $\alpha(Z\alpha)^{n \geq 3}$ for $Z = 92$ with nuclear radius $r_n = 5.751$ fm. Calculations were performed in the B-spline basis. Dashed lines: contributions from different κ ; solid line: sum over the first five contributions from different κ .

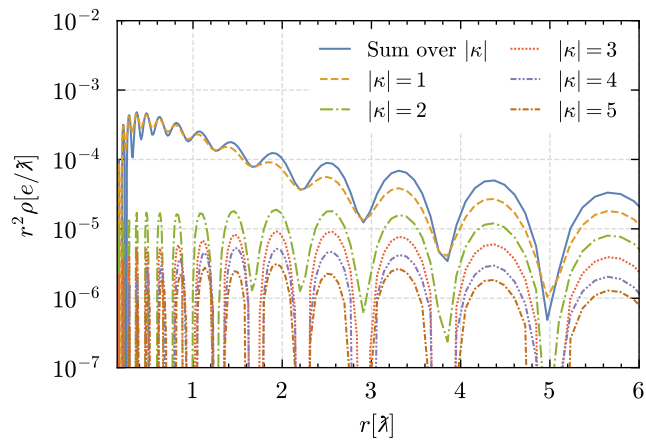


Figure 7. Same as Fig. 6, but in log-scale.

energy spectrum. We calculate this correction to test the accuracy of our VP charge density calculations and analyze the applicability of the proposed method to the Wichmann-Kroll correction calculations. As we have shown in Section IV A, a Gaussian basis set used for VP calculations provides better results, and therefore, we use these basis functions to calculate the Wichmann-Kroll energy corrections. The major part of the energy shift caused by the vacuum polarization comes from the $Z\alpha$ -order correction associated with the Uehling potential (see, for example, [13]). The correction originating from the higher orders is called the Wichmann-Kroll correction [14], and it can be calculated using $\rho^{n \geq 3}$. The potential created by this charge density is [1]:

$$V(r) = -4\pi\alpha \left[\frac{1}{r} \int_0^r \rho(r') r'^2 dr' + \int_r^\infty \rho(r') r' dr' \right], \quad (51)$$

from which, using (13), we can find the energy correction

for the electron with quantum numbers n and κ :

$$\begin{aligned} \Delta E_{\kappa,n} &= \int \varphi_{\kappa,n}^\dagger(r) V(r) \varphi_{\kappa,n}(r) dr = \\ &= \int V(r) (P_{n,\kappa}^2 + Q_{n,\kappa}^2) dr = \langle n, \kappa | V | n, \kappa \rangle \end{aligned} \quad (52)$$

Since the VP charge density can be expanded into different angular momentum contributions (36), these terms contribute to individual energy corrections terms, which are summed to obtain the total value:

$$\Delta E_n = \sum_{\kappa} \Delta E_{\kappa,n} \quad (53)$$

Because this value converges quite fast with increasing $|\kappa|$, we can take only the first few values of $\Delta E_{\kappa,n}$ to get accurate results (an extrapolation can be used [13], but the precision of our method is not high enough for us to consider this improvement). In this paper, we consider the first 5 terms in $|\kappa|$.

To compare the FBS approach for the calculation of the VP charge density with the traditional ones, we also performed calculations using a standard approach based on integration of Green's functions (see, for example, [1]). In Table II, we show the results for Wichmann-Kroll correction components for different $|\kappa|$, calculated with standard Green's function integration and using the FBS approximation with Gaussian basis sets of sizes 30 and 100. The calculations were performed for hydrogen-like Uranium with $Z = 92$, $r_n = 5.751$ fm, using the shell nucleus model (50). For higher $|\kappa|$, the corresponding terms should converge, but for the FBS calculation, the oscillations become considerable; therefore, higher κ terms vanish slower than they should, which adds to the error of the FBS method. Moreover, from Table II, we can see that the correction value converges to the value calculated by the integration method with increasing size of the basis set.

Table II. Contributions from different κ to the Wichmann-Kroll correction and their sum for 1s electron in hydrogen-like Uranium for different calculation methods. In parentheses, the difference between the corrections calculated by FBS and Green's function integration methods is shown.

$ \kappa $	$\Delta E_{\text{WK}} (\Delta E_{\text{WK}}^{\text{FBS}} - \Delta E_{\text{WK}}^{\text{Green}}), \text{ eV}$		
	Green's integr.	FBS $n = 30$	FBS $n = 100$
1	4.473	4.479 (0.006)	4.489 (0.016)
2	0.394	0.467 (0.073)	0.405 (0.011)
3	0.081	0.145 (0.064)	0.089 (0.008)
4	0.024	0.059 (0.035)	0.032 (0.008)
5	0.009	0.046 (0.037)	0.018 (0.009)
Sum	4.99	5.198 (0.208)	5.033 (0.043)

Further, we calculated Wichmann-Kroll corrections for the first few electron orbitals of several elements. The results are presented in Tables III and IV. We compare

our results with [13]. As can be seen from these tables, the FBS calculations provide results with a considerable error compared to the results from [13]. However, for the first two orbitals ($1s_{1/2}$, $2s_{1/2}$), our method gives results with error $\lesssim 10\%$ for the basis set size $n = 30$ and $\lesssim 3\%$ for the basis set size $n = 100$. Again, similar to Table II, the error decreases with increasing size of the basis set. In Table IV, we show only calculations with $n = 100$, since for the basis set with $n = 30$, the error here is too high.

V. DISCUSSION AND CONCLUSION

In this study, we have calculated vacuum polarization (VP) charge densities for several heavy hydrogen-like ions using the finite basis set approximation. Furthermore, we have calculated the Wichmann-Kroll corrections for the first few electron orbitals using these densities. As we show, the calculated charge densities are in good agreement with the results of Soff and Mohr [1, 21] for $|\kappa| = 1$. However, this method is subject to oscillation issues (see Figs. 2-7), which spoil the results for higher $|\kappa|$ and impose limitations on this calculation method. Conversely, the results become more reliable with larger basis sets. This method can be used to obtain good estimates for VP calculations, or as an independent approximate test for calculations performed by other methods, such as Green's function integration, and can be further improved by optimizing the computation algorithm to use larger basis sets more efficiently or by finding more suitable basis sets.

We have calculated the VP charge density using the Gaussian and B-spline basis sets, showing that for this task, the Gaussian basis provides good results (confirming the calculations from [17] for $|\kappa| = 1$), while B-spline calculations suffer from strong oscillations.

On the other hand, we certainly do not state that B-splines cannot be used for vacuum polarization calculations: we only show that this basis performs worse than the Gaussian one if the same approach is used. In principle, by using arbitrary precision or mixed basis sets, B-splines could be applied in VP calculation problems, but this matter should be investigated separately.

A known problem with Gaussian basis sets is linear

dependence, which imposes a limit on the maximum size of the basis set. This limitation can be lifted using arbitrary (multiple) precision computation methods. The presented results for the Wichmann-Kroll corrections show the convergence of the finite basis set approximation method with increasing size of the basis set. Such calculations are much slower than standard float-number calculations, but they are necessary for accurate results when using a large basis set. While calculations with float-numbers are imprecise (see Tables III and IV), they are extremely fast. Our code provides the result in about 2 seconds. This makes the proposed method a good benchmark for testing solutions obtained with time-consuming conventional approaches.

We conclude that the finite basis approximation method can be successfully used to calculate the Wichmann-Kroll energy corrections, if one is content with an accuracy within a few percent ($\lesssim 3\%$ for a Gaussian basis set with a size of $n = 100$ for $1s_{1/2}$ and $2s_{1/2}$ electrons in hydrogen-like heavy ions). We also believe that the accuracy of this method can be improved further, and it could be used in various atomic problems, such as evaluation of the higher orders of the Wichmann-Kroll correction or screening effects in lithium-like ions.

ACKNOWLEDGMENTS

We are grateful to I. Terekhov for criticism. We also deeply appreciate the discussion with M. Salman, who helped to clarify some important details in their paper and gave us useful computation tips. The authors thank L. Pogorelskaya for her proofreading of the English manuscript.

The studies in Sec. II are supported by the Foundation for the Advancement of Theoretical Physics and Mathematics "BASIS". The studies in Sec. III are supported by the Ministry of Science and Higher Education of the Russian Federation (Agreement No. 075-15-2021-1349). The studies in Sec. IV are supported by the Russian Science Foundation (Grant No. 22-12-00258; [34]).

-
- [1] P. J. Mohr, G. Plunien, and G. Soff, *Physics Reports* **293**, 227 (1998).
 - [2] V. A. Yerokhin, K. Pachucki, and V. Patkóš, *Annalen der Physik* **531**, 1800324 (2019).
 - [3] S. G. Karshenboim, V. G. Ivanov, and V. M. Shabaev, *Journal of Experimental and Theoretical Physics* **93**, 477 (2001).
 - [4] V. A. Yerokhin, C. H. Keitel, and Z. Harman, *Journal of Physics B: Atomic, Molecular and Optical Physics* **46**, 245002 (2013).
 - [5] N. A. Belov, B. Sikora, R. Weis, V. A. Yerokhin, S. Sturm, K. Blaum, C. H. Keitel, and Z. Harman, "Muonic vacuum polarization correction to the bound-electron g -factor," (2016), [arXiv:1610.01340](https://arxiv.org/abs/1610.01340) [[physics.atom-ph](https://arxiv.org/abs/1610.01340)].
 - [6] E. Dizer and Z. Harman, *Phys. Rev. A* **108**, 042808 (2023).
 - [7] A. V. Volotka, D. A. Glazov, G. Plunien, and V. M. Shabaev, *Annalen der Physik* **525**, 636 (2013).
 - [8] S. Sturm, F. Köhler, J. Zatorski, A. Wagner, Z. Harman, G. Werth, W. Quint, C. Keitel, and K. Blaum, *Nature* **506** (2014), 10.1038/nature13026.

Table III. Wichmann-Kroll vacuum polarization effects, calculated using FBS method for various elements, in eV, and error $(\Delta E_{\text{FBS}} - \Delta E_{\text{Persson}})/\Delta E_{\text{Persson}}$, %. For comparison, results from Persson et al. (1993) [13] are given. Calculations were made with basis set sizes $n = 30$ and $n = 100$. The nuclear radii of the elements are 5.273, 5.505, 5.860, and 5.976 fm, respectively. Here, $1s_{1/2}$ and $2s_{1/2}$ orbitals are considered.

	$1s_{1/2}$			$2s_{1/2}$		
	FBS n=30	FBS n=100	Persson(1993)	FBS n=30	FBS n=100	Persson(1993)
^{70}Yb	0.8462 (2.16%)	0.8375 (1.10%)	0.8283	0.1339 (11.77%)	0.1236 (3.17%)	0.1198
^{82}Pb	2.3575 (2.95%)	2.3087 (0.82%)	2.2900	0.3850 (8.94%)	0.3576 (1.19%)	0.3534
^{92}U	5.1982 (4.25%)	5.0332 (0.94%)	4.9863	0.8381 (2.03%)	0.8293 (0.96%)	0.8214
^{100}Fm	9.378 (3.41%)	9.1108 (0.46%)	9.069	1.684 (6.11%)	1.5964 (0.59%)	1.587

Table IV. Wichmann-Kroll corrections, calculated using FBS method for various elements, in eV, and error $(\Delta E_{\text{FBS}} - \Delta E_{\text{Persson}})/\Delta E_{\text{Persson}}$, %. For comparison, results from Persson et al. (1993) [13] are given. Calculations made with basis set size $n = 100$. The nuclear radii are the same as in Table III. Here, $2p_{1/2}$ and $2p_{3/2}$ orbitals are considered.

	$2p_{1/2}$		$2p_{3/2}$	
	FBS n=100	Persson(1993)	FBS n=100	Persson(1993)
^{70}Yb	0.0170 (11.11%)	0.0153	0.0041 (46.43%)	0.0028
^{82}Pb	0.0698 (5.76%)	0.0660	0.0120 (27.66%)	0.0094
^{92}U	0.2138 (3.94%)	0.2057	0.0269 (19.03%)	0.0226
^{100}Fm	0.5091 (2.23%)	0.498	0.0497 (15.58%)	0.043

- [9] V. M. Shabaev, D. A. Glazov, N. S. Oreshkina, A. V. Volotka, G. Plunien, H.-J. Kluge, and W. Quint, *Phys. Rev. Lett.* **96**, 253002 (2006).
- [10] V. A. Yerokhin, E. Berseneva, Z. Harman, I. I. Tupitsyn, and C. H. Keitel, *Phys. Rev. Lett.* **116**, 100801 (2016).
- [11] A. N. Artemyev, V. M. Shabaev, and V. A. Yerokhin, *Phys. Rev. A* **56**, 3529 (1997).
- [12] A. V. Malyshev, A. V. Volotka, D. A. Glazov, I. I. Tupitsyn, V. M. Shabaev, and G. Plunien, *Phys. Rev. A* **90**, 062517 (2014).
- [13] H. Persson, I. Lindgren, S. Salomonson, and P. Sunnergren, *Phys. Rev. A* **48**, 2772 (1993).
- [14] E. H. Wichmann and N. M. Kroll, *Phys. Rev.* **101**, 843 (1956).
- [15] M. Gyulassy, *Phys. Rev. Lett.* **33**, 921 (1974).
- [16] V. M. Shabaev, I. I. Tupitsyn, V. A. Yerokhin, G. Plunien, and G. Soff, *Phys. Rev. Lett.* **93**, 130405 (2004).
- [17] M. Salman and T. Saue, *Phys. Rev. A* **108**, 012808 (2023).
- [18] V. B. Berestetskii, E. M. Lifshitz, and L. P. Pitaevskii, *Quantum electrodynamics*, Course of Theoretical Physics, Vol. 4 (Pergamon Press, Oxford, UK, 1982).
- [19] I. Grant, *Relativistic Quantum Theory of Atoms and Molecules: Theory and Computation*, Springer Series on Atomic, Optical, and Plasma Physics (Springer New York, 2007).
- [20] J. Schwinger, *Phys. Rev.* **82**, 664 (1951).
- [21] G. Soff and P. J. Mohr, *Phys. Rev. A* **38**, 5066 (1988).
- [22] I. P. Grant, *Journal of Physics B: Atomic and Molecular Physics* **19**, 3187 (1986).
- [23] I. P. Grant and H. M. Quiney, *Phys. Rev. A* **62**, 022508 (2000).
- [24] W. R. Johnson, S. A. Blundell, and J. Sapirstein, *Phys. Rev. A* **37**, 307 (1988).
- [25] J. Sapirstein and W. Johnson, *Journal of Physics B-atomic Molecular and Optical Physics - J PHYS-B-AT MOL OPT PHYS* **29**, 5213 (1996).
- [26] G. W. F. Drake and S. P. Goldman, *Phys. Rev. A* **23**, 2093 (1981).
- [27] There is an important feature of eigenvectors, sometimes called **B**-orthogonality. This means that if in a $\mathbf{A}\mathbf{v} = \lambda\mathbf{B}\mathbf{v}$ problem, the matrices **A** and **B** are both symmetric or Hermitian, and if **B** is a positive-definite matrix, then $\mathbf{v}_i^T \mathbf{B} \mathbf{v}_j = \delta_{ij}$, or, in our notation, $\mathbf{v}_i^T \mathbf{C} \mathbf{v}_j = \delta_{ij}$. Here we must note that since eigenvectors are defined up to a constant factor, they can vary for different calculation methods and programs; as a result, diagonal elements on the right side in the equations above can differ from one. Methods like DSYGV return such eigenvectors, which give δ_{ij} in the **B**-orthogonality relations. This property allows control over the calculation precision, since in numerical calculation, one would see $\mathbf{v}_i^T \mathbf{C} \mathbf{v}_i = 1 \pm \epsilon$, where ϵ is a small number, which become larger if the solution error increases.
- [28] I. I. Tupitsyn and V. M. Shabaev, *Optics and Spectroscopy* **105**, 183 (2008).
- [29] G. A. Rinker and L. Wilets, *Phys. Rev. A* **12**, 748 (1975).
- [30] C. de Boor, *A Practical Guide to Spline*, Vol. Volume 27 (1978).
- [31] I. P. Grant and H. M. Quiney, *Advances in atomic and molecular physics* **23**, 37 (1988).
- [32] The mpmath development team, *mpmath: a Python library for arbitrary-precision floating-point arithmetic (version 1.3.0)* (2023), <http://mpmath.org/>.
- [33] We note that the evaluation time can be reduced by choosing a smaller grid, less digit numbers or by over-all optimizing the calculation algorithm, which was not our main goal in current work.
- [34] <https://rscf.ru/en/project/22-12-00258/>.